Hydrological Processes in Regional Climate Model Simulations of the Central United States Flood of June–July 1993

CHRISTOPHER J. ANDERSON,[a] RAYMOND W. ARRITT,[a] EUGENE S. TAKLE,[a,b] ZAITAO PAN,[a] WILLIAM J. GUTOWSKI JR.,[a,b] FRANCIS O. OTIENO,[b] RENATO DA SILVA,[o] DANIEL CAYA,[h] JENS H. CHRISTENSEN,[d] DANIEL LÜTHI,[l] MIGUEL A. GAERTNER,[m] CLEMENTE GALLARDO,[m] FILIPPO GIORGI,[j] SONG-YOU HONG,[p] COLIN JONES,[k] H.-M. H. JUANG,[e] J. J. KATZFEY,[c] WILLIAM M. LAPENTA,[g] RENÉ LAPRISE,[j] JAY W. LARSON,[n] GLEN E. LISTON,[i] JOHN L. MCGREGOR,[c] ROGER A. PIELKE SR.,[i] JOHN O. ROADS,[f] AND JOHN A. TAYLOR[n]

[a]*Department of Agronomy, Iowa State University, Ames, Iowa*
[b]*Department of Geological and Atmospheric Sciences, Iowa State University, Ames, Iowa*
[c]*Commonwealth Scientific and Industrial Research Organisation, Aspendale, Australia*
[d]*Danish Meteorological Institute, Copenhagen, Denmark*
[e]*National Centers for Environmental Prediction, Camp Springs, Maryland*
[f]*Scripps Institution of Oceanography, La Jolla, California*
[g]*Marshall Space Flight Center, Huntsville, Alabama*
[h]*Department of Earth and Atmospheric Sciences, Université du Québec á Montréal, Montreal, Quebec, Canada*
[i]*Department of Atmospheric Science, Colorado State University, Fort Collins, Colorado*
[j]*International Center for Theoretical Physics, Trieste, Italy*
[k]*Rossby Center at the Swedish Meteorological and Hydrological Institute, Norrkoping, Sweden*
[l]*Swiss Federal Institute of Technology (ETH), Zurich, Switzerland*
[m]*Environmental Sciences Faculty, Universidad de Castilla-La Mancha, Toledo, Spain*
[n]*Mathematics and Computer Science Division, Argonne National Laboratory, Argonne, Illinois*
[o]*Department of Civil and Environmental Engineering, Duke University, Durham, North Carolina*
[p]*Department of Atmospheric Sciences, Yonsei University, Seoul, South Korea*

(Manuscript received 9 April 2002, in final form 4 December 2002)

ABSTRACT

Thirteen regional climate model (RCM) simulations of June–July 1993 were compared with each other and observations. Water vapor conservation and precipitation characteristics in each RCM were examined for a 10° × 10° subregion of the upper Mississippi River basin, containing the region of maximum 60-day accumulated precipitation in all RCMs and station reports.

All RCMs produced positive precipitation minus evapotranspiration ($P - E > 0$), though most RCMs produced $P - E$ below the observed range. RCM recycling ratios were within the range estimated from observations. No evidence of common errors of E was found. In contrast, common dry bias of P was found in the simulations.

Daily cycles of terms in the water vapor conservation equation were qualitatively similar in most RCMs. Nocturnal maximums of P and C (convergence) occurred in 9 of 13 RCMs, consistent with observations. Three of the four driest simulations failed to couple P and C overnight, producing afternoon maximum P. Further, dry simulations tended to produce a larger fraction of their 60-day accumulated precipitation from low 3-h totals.

In station reports, accumulation from high (low) 3-h totals had a nocturnal (early morning) maximum. This time lag occurred, in part, because many mesoscale convective systems had reached peak intensity overnight and had declined in intensity by early morning. None of the RCMs contained such a time lag. It is recommended that short-period experiments be performed to examine the ability of RCMs to simulate mesoscale convective systems prior to generating long-period simulations for hydroclimatology.

1. Introduction

Mesoscale processes and regional surface conditions influence the water cycle of the central United States (Rasmusson 1967; Fritsch et al. 1986; Higgins et al. 1997), suggesting that high-resolution models are necessary for detailed, physically based simulation of the region's hydroclimate. One approach to this problem is the use of a regional climate model (RCM) that nests a high-resolution limited-area model within the grid of a coarser-resolution analysis or climate model. A variety of RCM architectures exist, but systematic comparison of output from different RCMs is lacking (Giorgi and Mearns 1999). In response to this need a number of

Corresponding author address: Christopher J. Anderson, Iowa State University, 3010 Agronomy Hall, Ames, IA 50011-1010.
E-mail: candersn@iastate.edu

groups have developed RCM intercomparison projects. RCM intercomparisons provide a common experimental framework to systematically identify processes that are simulated well or poorly, thereby either increasing confidence in RCMs as prognostic tools or indicating model components in need of improvement (Takle et al. 1999).

In the present study results from 13 RCMs that participated in experiment 1b of the Project to Intercompare Regional Climate Simulations (PIRCS; Gutowski et al. 1998; Takle et al. 1999) are compared with each other and observations. The 60-day simulation period spans 1 June–31 July 1993, overlapping the peak precipitation episode of the central United States flood (Arritt et al. 1997). It is well documented that an unusually high incidence of heavy precipitation, mesoscale convective systems (MCSs) and low-level jets (LLJs) contributed to this flood event (Kunkel et al. 1994; Arritt et al. 1997; Anderson and Arritt 1998). These mesosocale processes are important not only to this event but also to hydroclimatology of the central United States (Fritsch et al. 1986; Higgins et al. 1997). The short period of simulation for PIRCS experiment 1b facilitates detailed examination of whether RCM output contains characteristics of such mesoscale weather elements. The ability of RCMs to reproduce mesoscale dynamics in the central United States has not been examined in much detail, so that, while it is well known that RCM output in regions of highly variable terrain is more reasonable when compared with GCM output (Seth and Giorgi 1998), it is unknown whether this may be said of RCM output in the central United States where the terrain is relatively flat.

In our intercomparison, we emphasize sources of systematic intermodel variability of precipitation, evapotranspiration, and horizontal moisture flux. The intercomparison focuses on a $10° \times 10°$ latitude–longitude box (37°–47°N, 99°–89°W) within the upper Mississippi River basin (UMRB; shown in Fig. 1). The location of 60-day maximum precipitation is contained within this region in all simulations and in the observations. The following section contains a description of data sources and methodology. Results follow in section 3, and a summary with discussion is given in section 4.

2. Data sources

a. Regional climate models

The RCMs examined herein[1] include six limited-area models developed outside the United States (DARLAM, CRCM, EM, HIRHAM, PROMES, SweCLIM), two adaptations of the fifth-generation Pennsylvania State University–National Center for Atmospheric Research (PSU–NCAR) Mesoscale Model MM5 (MM5–ANL, MM5–BATS), a regional climate adaptation of PSU–NCAR MM4 model (RegCM2), and two spectral models (NCEP RSM, Scripps RSM). Selected characteristics of the 13 limited-area models used in this study are listed in Tables 1 and 2. The continental United States and portions of adjacent oceans were included in the domain of each RCM. The nominal node spacing was 50 km but varied slightly in each RCM because of different map projections. Each simulation ran continuously from initialization on 1 June 1993 with lateral boundaries updated at 6-h intervals. Additional details of the PIRCS experimental design are reported in Takle et al. (1999).

Initial and boundary data (including soil moisture) were generated from the NCEP–NCAR reanalysis and were made accessible to each modeling group by PIRCS. Each group was responsible for interpolating this data onto the group's model's computational grid. For three RCMs (EM, PROMES, SweCLIM-ECMWF), initial and boundary data were derived from the European Centre for Medium-Range Weather Forecasts (ECMWF) reanalysis. Note that our intercomparison includes two simulations from SweCLIM (SweCLIM-NCEP, SweCLIM-ECMWF) that differ only in the source of initial and boundary conditions. The nesting strategy for NCEP RSM and Scripps RSM differs markedly from the other limited-area models in that both models use information from the reanalysis over the inner domain as well as near the lateral boundaries through domain nesting (Juang and Kanamitsu 1994; Juang et al. 1997; Juang and Hong 2001). The two RSM implementations differ only in the convective parameterization scheme. In addition to differences of lateral boundary data source, climatological soil moisture conditions were used in CRCM. Since the domain of all RCMs extends over adjacent oceans where data is limited in comparison with the United States, our results may be sensitive to the source of initial and boundary data.

b. Observed precipitation

Precipitation observations used in this study include station hourly precipitation, gridded hourly precipitation (Higgins et al. 1996), and gridded monthly precipitation (Legates and Willmot 1990). We derived station hourly precipitation from the hourly precipitation data (HPD)

[1] DARLAM—Commonwealth Science and Industrial Research Organisation Division of Atmospheric Research Limited Area Model; CRCM—University of Québec at Montreal Canadian Regional Climate Model; EM—Swiss Federal Institute of Technology Climate High-Resolution Model; HIRHAM—High-Resolution Hamburg climate model; PROMES—University of Complutense in Madrid regional climate model; RegCM2—National Center for Atmospheric Research Regional Climate Model version 2; SweCLIM—Swedish Meteorological and Hydrological Institute regional climate model; MM5–ANL—MM5 version 3; MM5–BATS—Biosphere–Atmosphere Transfer Scheme coupled to MM5; NCEP RSM—National Centers for Environmental Prediction Regional Spectral Model; Scripps RSM—Scripps regional spectral model.

TABLE 1. Characteristics of models selected from PIRCS experiment 1b.

Model	Investigator	Grid[a]	Levels	Dynamics[b]	Lateral[c] boundary condition	Reference
ClimRAMS	Liston, Pielke	PS	20	NON	PAR/10	Pielke et al. (1992), Liston and Pielke (2001)
CRCM	Caya, Laprise	PS	20	NON	DIF/9	Caya and Laprise (1999)
DARLAM	McGregor, Katzfey	LC	18	HYD	EXP/10	McGregor et al. (1993b), McGregor and Walsh (1994)
EM	Lüthi	AC	20	HYD	DIF/9	Lüthi et al. (1996)
HIRHAM	Christiansen, Lopez	MER	19	HYD	EXP/10	Christensen et al. (1997)
MM5–ANL	Taylor	LC	23	NON	LIN/4	Taylor and Larson (2001)
MM5–BATS	Lapenta	LC	32	NON	LIN/4	Grell et al. (1993), Lakhtakia and Warner (1994)
NCEP RSM	Hong	PS	28	HYD	EXP/10	Juang et al. (1997), Hong (2000)
PROMES	Gaertner	LC	26	HYD	LIN/8	Gaertner et al. (2001)
RegCM2	Pan	LC	14	HYD	EXP/10	Giorgi et al. (1993a), Giorgi et al. (1993b)
Scripps RSM	Roads, Chen	MER	28	HYD	EXP/10	Juang and Kanamitsu (1994)
SweCLIM	Jones	RLL	19	HYD	TANH/8	Jones and Willen (2001)

[a] Horizontal grid types: AC, Arakawa-C; RLL, rotated latitude–longitude; MER, Mercator (lat–lon); PS, polar stereographic; LC, Lambert conformal.
[b] Dynamics: HYD, hydrostatic; NON, nonhydrostatic.
[c] Lateral boundary condition: weighting function used blending large-scale and internal tendencies [LIN, linear decrease toward center of domain; EXP, exponential decrease; PAR, parabolic decrease; TANH, hyperbolic tangent profiles; DIF, dynamical diffusion following Davies (1976)] and number of grid points in the blending region.

archive at the National Climatic Data Center (NCDC). Most station reports in the HPD had precision of 2.54 mm, but some reported precipitation to 0.254 mm. For consistency, we truncated the latter to 2.54 mm. Quality control procedures at NCDC removed stations that consistently failed to report both temperature and precipitation. We applied additional selection criteria, removing station records with gaps $\geq$24 consecutive hours. The dataset used in this analysis contains 242 stations within the UMRB box. Domain-average precipitation was the arithmetic mean of precipitation at stations within the UMRB box.

c. Diagnostic quantities

Model output used to compute diagnostic quantities includes evaporation, precipitation, precipitable water, specific humidity, and u- and v-wind components. Quantities that involved mathematical operations of these variables, such as water vapor transport (the product of specific humidity and u- and v-wind components) or accumulated precipitation, were computed on the native lattice of each RCM. In order to facilitate direct comparison of RCM output, however, a common grid must be used. We interpolated all diagnostic quantities to a common 0.5° × 0.5° lat–lon grid, which is approximately the nominal node spacing of the RCMs. We used a single-pass Barnes scheme (Barnes 1964) with e-folding distance set to 0.5° in order to damp signals less than twice the analysis grid spacing.

1) WATER VAPOR CONSERVATION EQUATION

Rasmusson (1968) and Peixoto and Oort (1992) have derived an area-average water vapor conservation equation,

$$S = (E + C) - P, \tag{1}$$

where S is the atmospheric water vapor storage, E is evapotranspiration rate, P is precipitation rate, and C is convergence of vertically integrated atmospheric water vapor flux. The terms S and C are

$$S = \frac{\partial}{\partial t}\int_{P_T}^{P_S} q\,\frac{dp}{g} \quad \text{and} \tag{2}$$

$$C = -\nabla \cdot \mathbf{Q}, \tag{3}$$

where g is the gravitation constant, q is specific humidity, p is pressure, and integration boundaries P_S and P_T are pressure at the surface and top of the atmosphere, respectively. The vertically integrated atmospheric water vapor flux, $\mathbf{Q}$, is

$$\mathbf{Q} = \int_{P_T}^{P_S} \mathbf{v}q\,\frac{dp}{g} \tag{4}$$

where $\mathbf{v}$ is the two-dimensional velocity vector. The right-hand side of (1) represents processes that can change the atmospheric water vapor content in a unit

TABLE 2. Parameterizations in models selected from PIRCS experiment 1b.

Model	Investigator	Land surface[a]	Boundary layer[b]	Explicit precipitation	Convection[c]
ClimRAMS	Liston, Pielke	BATS	Local K: gradient-Richardson	Rain and ice physics: prognostic cloud water	KA
CRCM	Caya, Laprise	Single-layer soil model vegetation	Local K: gradient-Richardson	Rain and ice physics: prognostic rain, cloud water	KF
DARLAM	McGregor, Katzfey	Soil water: six-layer temperature: six-layer vegetation	Local K: gradient-Richardson	Rain physics: prognostic water vapor	AG
EM	Lüthi	Three-layer soil model vegetation	Second-order Mellor and Yamada	Rain and ice physics: prognostic cloud water	MF
HIRHAM	Christiansen, Lopez	Soil water: one-layer temperature: five-layer vegetation	1.5-order closure, local K: prognostic TKE	Rain and ice physics: prognostic cloud water	MF
MM5–ANL	Taylor	OSU	Blackadar	Rain and ice physics: prognostic cloud water	Grell
MM5–BATS	Lapenta	BATS	MRF	Rain and ice physics: prognostic cloud water	Grell
NCEP RSM	Hong	Soil water: two-layer temperature: two-layer vegetation	Nonlocal eddy flux: Holtslag et al. (1990)	Rain physics: prognostic water vapor	Modified PW
PROMES	Gaertner	Soil water: two-layer temperature: two-layer vegetation	Local K: Blackadar coefficients	Rain physics: prognostic rain, cloud water	KF
RegCM2	Pan	BATS	Nonlocal eddy flux: Holtslag et al. (1990)	Rain physics: prognostic cloud water	Grell
Scripps RSM	Roads, Chen	Soil water: two-layer temperature: two-layer vegetation	Nonlocal eddy flux: Troen and Mahrt (1987)	Rain physics: prognostic water vapor	PW
SweCLIM	Jones	Soil water: two-layer temperature: two-layer vegetation	Local K: prognostic TKE	Rain and ice physics: prognostic cloud water	KF

[a] Land surface scheme: BATS, Biosphere–Atmosphere Transfer Scheme, five-layer soil model, Dickinson et al. (1993); OSU, Oregon State University, multilayer soil model, Chen and Dudhia (2001).
[b] Boundary-layer scheme: MRF, Medium Range Forecast model, nonlocal eddy flux, Troen and Mahrt (1987), Hong and Pan (1996); Blackadar, local K, gradient-Richardson, Zhang and Anthes (1982).
[c] Convection scheme: AS, Arakawa–Schubert, Arakawa and Schubert (1974); AG, Arakawa–Gordon, McGregor et al. (1993a); Grell, Grell et al. (1993) and Grell (1993); MF, mass flux scheme following Tiedtke (1989); KA, Kuo (1974); KF, Kain–Fritsch, Kain and Fritsch (1990); PW, Pan-Wu, Pan and Wu (1995).

column. In this formalism, conversion to and from suspended liquid water and ice is neglected.

We applied the water vapor conservation equation (1) to the UMRB box for the 60-day period of the PIRCS simulations. Output from all RCMs included 3-h accumulation of precipitation and surface latent heat flux, so that P and E in (1) were specified completely by dividing the 3-h accumulation by 3 h and averaging over all 3-h periods. Output from most PIRCS RCMs included instantaneous precipitable water every 3 h, but for those that did not we computed instantaneous precipitable water every 6 h from instantaneous values of q and p. The difference of precipitable water between successive 3- or 6-h periods divided by the respective time period was the precipitable water tendency. The 60-day average storage (S) was the average of precipitable water tendency taken over each 3- or 6-h interval. All time averages were computed on the native grid of each RCM, that is, prior to interpolation. Domain averages were the arithmetic mean of interpolated water vapor conservation components at each grid point within the UMRB boundaries.

Estimates of water vapor convergence in the central United States are sensitive to the frequency and spatial density of wind reports (Berbery and Rasmusson 1999), due to nocturnal acceleration of the low-level wind field over this region (Rasmusson 1968; Berbery and Rasmusson 1999). Since horizontal node spacing of the RCM output is approximately 50 km $\times$ 50 km, horizontal resolution should not be a large source of error in convergence estimates, although some error is introduced during interpolation. However, PIRCS models archived wind components 4 times per day, which is half the frequency recommended by Berbery and Rasmusson (1999). This limitation was a consequence of mass-storage capacity.

Equation (3) may be reformulated by use of Gauss's theorem as

$$C^* = \oint \mathbf{Q} \cdot \mathbf{n}\, d\gamma, \tag{5}$$

where $\mathbf{n}$ is the unit vector normal to the perimeter and γ is a unit length along the perimeter. We computed the

line integral along the perimeter of the UMRB box of the 60-day average of vertically integrated water vapor flux. The error, Δ, of C^* was

$$\Delta = C - C^*, \tag{6}$$

where C is computed by rearranging the water vapor conservation equation (1). Typical values of Δ were less than 30% of the magnitude of C^*. It is impossible to separate the contribution to Δ by specific error sources, such as smoothing and undersampling of the wind field. However, Δ of this magnitude is consistent with accuracy estimates for observed water vapor convergence in this region (Gutowski et al. 1997). In a few RCMs Δ was as large as twice the magnitude of C (DARLAM, MM5–ANL, MM5–BATS, RegCM2). We have found a high incidence of LLJs (not shown) in RCMs that are based on the PSU–NCAR Mesoscale Model (including RegCM2) relative to that of other RCMs in our collection. This result in conjunction with large Δ suggests the low-level wind experiences a dramatic nocturnal acceleration that might require more frequent sampling in order to characterize C^* accurately. Because of this disparity and since model P, E, and S are well represented in model output, we examined C as a residual rather than C^*.

2) WATER VAPOR FLUX

The unique nocturnal maximum of summertime precipitation in the U.S. midwest (Wallace 1975) temporally separates the daily maxima of P and E. This diurnal pattern, coupled with the nocturnal maximum of LLJs, raises questions about the diurnal cycle of water vapor flux in this region. To account for sampling errors discussed in the previous section, we applied an adjustment to the 60-day averages of water vapor influx and efflux. The total influx, F_{in}, (or efflux, F_{out}) of water vapor was the line integral along the perimeter of the UMRB box for which the 60-day average of $\mathbf{Q}$ was directed inward (or outward). We adjusted F_{in} and F_{out} as follows:

$$F'_{in} = F_{in} + 0.5\Delta \tag{7}$$

$$F'_{out} = F_{out} - 0.5\Delta. \tag{8}$$

3) RECYCLING RATIO

Estimates of water cycling in the central United States indicate that a small fraction of this region's precipitation originates as evaporated water vapor from within the region itself (Brubaker et al. 1993; Trenberth 1999). This characteristic is used as a gross diagnostic of the atmospheric hydrologic cycle in the PIRCS RCMs. A common quantification of water cycling is the two-dimensional recycling ratio ρ derived by Brubaker et al. (1993), which has the form

$$\rho = \frac{E'A}{E'A + 2F_{in}}, \tag{9}$$

where E' is area-average evapotranspiration, A is area, and F_{in} is water vapor influx. We computed ρ for each RCM using 60-day averages of E' and F_{in}. We computed ρ with F'_{in} substituted for F_{in} and found the difference to be inconsequential. The two-dimensional recycling ratio (for a complete review of recycling models see Burde and Zangvil 2001) was formulated for linearly varying fields under the assumption of a well-mixed atmosphere in steady state. If these assumptions were strictly met, the fraction of precipitation from evaporated water vapor within the domain would be exactly quantified. In the central U.S. LLJs, transient synoptic-scale low-pressure systems, spatial heterogeneity of P and E, and temporal coherence between LLJs and precipitation are a few of many conditions that may violate these assumptions (Trenberth 1999; Burde and Zangvil 2001). Therefore, we suggest a cautious interpretation, following Trenberth (1999), in which ρ is considered an index rather than an exact measure of recycling.

3. Results

a. Precipitation

Observed accumulated precipitation for June–July 1993, as estimated by using data from an archive initiated by Legates and Willmot (1990), exceeds 400 mm over Iowa, north-central and northeastern Kansas, northern Missouri, southeast Nebraska, and southwest Minnesota (Fig. 1a). Maxima exceeding 550 mm are located in north-central Kansas and central Iowa. The spatial pattern closely resembles a smoothed contour analysis of rain gauge data for June–August 1993 (Kunkel et al. 1994). The NCEP–NCAR reanalysis produces maximum precipitation exceeding 550 mm in eastern Iowa (Fig. 1b).

All RCMs produced maximum precipitation within the central United States, ranging from about 325 to just over 700 mm. Within this wide range, eight RCMs (HIRHAM, MM5–ANL, MM5–BATS, NCEP RSM, PROMES, RegCM2, Scripps RSM, SweCLIM-ECMWF) produced maximum precipitation between 450 and 650 mm. RCM precipitation averaged over all models exceeds 300 mm in an area covering Iowa, southeast Minnesota, and western Wisconsin (Fig. 1c). This northeastward displacement of maximum composite precipitation compared with maximum observed precipitation reflects an error of spatial location that occurs in all RCMs except ClimRAMS, CRCM, and PROMES (precipitation plots for each RCM are available online at www.pircs.iastate.edu/hydrology/precipitation.html). The much lower maximum in composite precipitation compared with observations has two causes. First, simulated maximum precipitation is less than observed maximum precipitation in the climate version of the Regional Atmospheric Modeling System (ClimRAMS), CRCM, MM5–ANL, SweCLIM-ECMWF, and SweCLIM-NCEP, whereas observed maximum precipitation

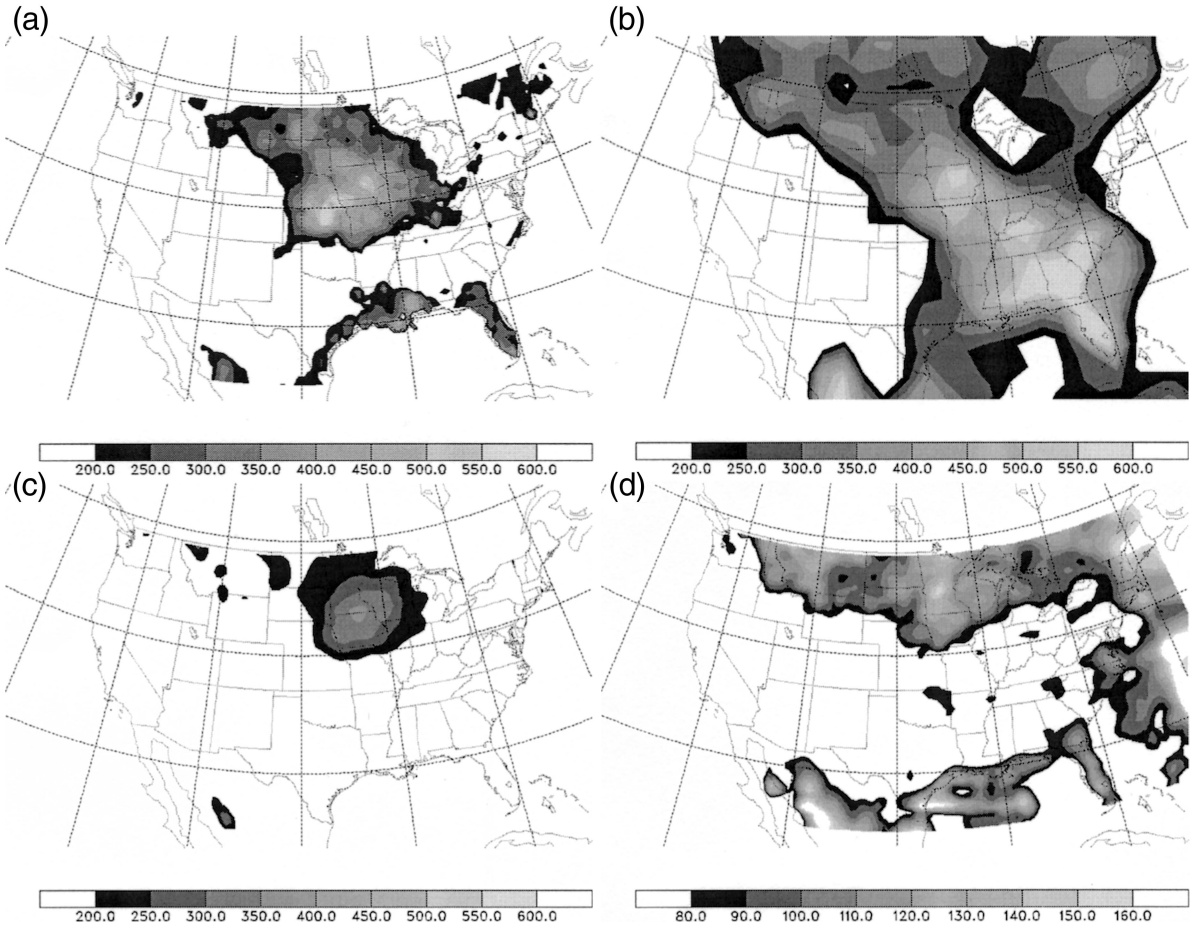

FIG. 1. Precipitation (mm) for Jun–Jul 1993 in (a) gridded observations, (b) NCEP–NCAR reanalysis, (c) RCM composite, and (d) standard deviation of RCM composite.

is exceeded only in EM and DARLAM. Second, the position of maximum 60-day precipitation varies markedly. Simulated 60-day precipitation maxima are located anywhere from northeastern Kansas to central Minnesota. These errors combine to produce an rmse that is as much as 50% (28%) of the composite (observed) maximum (Fig. 1d).

Position errors may be caused by inadequate representation of unresolved processes in RCMs (such as subgrid precipitation and turbulence) or errors of large-scale and transient synoptic conditions that propagate into the RCM interior domain from the boundary data. A comparison of SweCLIM-ECMWF with SweCLIM-NCEP gives direct evidence of the influence of boundary data, although it cannot be assumed that all other RCMs would respond to alternative boundary data in exactly the same way. Simulated precipitation exceeding 400 mm in SweCLIM-ECMWF extends from western Iowa northward into central Minnesota, while in SweCLIM-NCEP it is confined to central Minnesota. Although the southern edge of maximum precipitation in SweCLIM-ECMWF is much closer to the observed maximum, heavy precipitation in this simulation over Minnesota is contradictory with the hypothesis that precipitation is significantly altered by biases of large-scale circulation in the boundary data source. We have also examined movies of 500-hPa geopotential height fields in both SweCLIM-ECMWF and SweCLIM-NCEP, which show small differences in patterns of transient synoptic-scale systems. Whereas different boundary conditions for the two SweCLIM simulations produced small differences in their precipitation fields, precipitation fields for the three RCMs that used boundary conditions from ECMWF reanalysis (EM, PROMES, SweCLIM-ECMWF) differ markedly from each other with maximum precipitation varying in magnitude from about 400 to over 650 mm and in location from central Minnesota to southwest Iowa. These results suggest that, in this intercomparison, if systematic differences of simulated precipitation fields were caused by using alternative lateral boundary data sources, the differences were overwhelmed by variability related to design of the limited-area model.

These results have led us to examine more closely

the RCMs themselves for systematic errors of precipitation. In most RCMs maximum accumulated precipitation occurred north of a near-surface potential temperature gradient in the 60-day average potential temperature field and downwind of maximum LLJ frequency. This suggests that frontal overrunning was a key mechanism in generating precipitation in many RCMs. Radar and satellite imagery indicate this was not the case for observed precipitation. We have viewed surface weather maps, radar summaries, and Geostationary Operational Environmental Satellite (*GOES-8*) infrared (IR) imagery and have found that observed precipitation frequently formed south of surface fronts, became organized as an MCS, and moved along or slightly north of the surface front. Further evidence that observed precipitation occurred along and south of surface fronts is given by Junker et al. (1999) who conclude that a significant fraction of precipitation in June–July 1993 was produced by ''regenerating convective cells moving along a stationary low-level boundary.'' Thus, systematic error of precipitation location in RCMs is likely related to an inability of these RCMs to simulate precipitation systems along and south of the mean potential temperature gradient.

b. RCM 60-day hydrology components

1) PRECIPITATION MINUS EVAPOTRANSPIRATION ($P - E$)

Over a climatological average, summertime E exceeds P in the central United States (Roads et al. 1994; Kunkel 1990; Gutowski et al. 1997). Positive $P - E$ in June–July 1993 was a large deviation from such a climatological norm. Estimated $P - E$ in May–June–July 1993 from global analyses or reanalyses was 2–3 mm day^{-1} (Trenberth and Guillemot 1996; Gutowski et al. 1997). Positive $P - E$ was produced in every RCM simulation, although values exceeded 2 mm day^{-1} only in DARLAM and PROMES (Table 3). Nine RCMs (ClimRAMS, EM, HIRHAM, MM5–ANL, MM5–BATS, NCEP RSM, SweCLIM-ECMWF, SweCLIM-NCEP, RegCM2) produced $P - E$ within the range 0.5 to 1.5 mm day^{-1}. The overall tendency to understate $P - E$ is due to low bias of P in 10 RCMs (ClimRAMS, CRCM, EM, HIRHAM, MM5–ANL, MM5–BATS, PROMES, SweCLIM-ECMWF, SweCLIM-NCEP, RegCM2). Only DARLAM produced P greater than observed.

TABLE 3. Terms from 60-day water vapor conservation equation (mm day^{-1}).

Model	S	E	P	C	$P - E$	ρ
ClimRAMS	0.4	3.5	4.0	0.9	0.5	N/A
CRCM	0.0	2.9	4.6	1.7	1.7	N/A
DARLAM	0.3	3.8	6.5	3.0	2.7	0.06
EM	0.5	4.2	5.0	1.3	0.8	0.06
HIRHAM	0.7	3.5	4.4	1.6	0.9	0.06
MM5–ANL	0.3	3.3	4.3	1.3	1.0	0.06
MM5–BATS	0.3	4.3	5.3	1.3	1.0	0.06
NCEP RSM	0.3	5.4	6.0	0.9	0.6	0.08
PROMES	0.1	2.0	5.1	3.2	3.1	0.03
RegCM2	0.4	3.8	5.2	1.8	1.4	0.07
Scripps RSM	0.3	5.6	5.9	0.6	0.3	0.08
SweCLIM-ECMWF	0.1	4.3	5.4	1.2	1.1	0.07
SweCLIM-NCEP	0.2	4.1	5.0	1.1	0.9	0.07
Observations						
Station	N/A	N/A	6.2	N/A	N/A	N/A
Higgin Grid	N/A	N/A	5.9	N/A	N/A	N/A
Delaware Grid	N/A	N/A	6.2	N/A	N/A	N/A

2) PRECIPITATION

Precipitation rate depends on water vapor supply at the RCM boundaries and on precipitation processes internal to the RCMs. It is likely that some differences of model P are attributable to differences in model lateral boundary placement and methods for assimilating lateral boundary data (Seth and Giorgi 1998; Hong and Pan 2000). Lateral boundary nudging-zone width and dynamic constraints are unique to each RCM. Furthermore, the NCEP RSM and Scripps RSM have a unique nesting strategy of a domain nesting in physical space as well as a spectral nesting in spectral space (Juang and Hong 2001). It is beyond the scope of PIRCS to quantify sensitivity of P to lateral boundary details for each RCM. We have, however, examined whether different boundary data sources are associated with systematic differences of P. In order to do so, we have divided the models into two subgroups: one contained three RCMs (EM, SweCLIM-ECMWF, PROMES) that were provided boundary conditions from the ECMWF reanalysis, and the other contained the remaining 10 RCMs (ClimRAMS, CRCM, DARLAM, ETH, HIRHAM, MM5–ANL, MM5–BATS, NCEP RSM, SweCLIM-NCEP, RegCM2) that were given boundary conditions from the NCEP–NCAR reanalysis. The range of P of the ECMWF group is contained within the range of P of the NCEP–NCAR group. In addition, the difference of P between SweCLIM-NCEP and SweCLIM-ECMWF is slightly less than the range of P in models based on the PSU–NCAR Mesoscale Model that were driven by boundary conditions generated from the NCEP–NCAR reanalysis (0.4 mm day^{-1} compared with 1.0 mm day^{-1}). Thus, we find no evidence that suggests systematic errors of P have resulted from different boundary conditions in this intercomparison, in agreement with the result for precipitation fields of section 3a. Note that North America is a data-rich region compared with much of the rest of the globe, so that differences between ECMWF and NCEP–NCAR reanalyses should be relatively small; thus, our result should not be extrapolated to other regions.

Water vapor supply through the lower boundary should relate to P as well. Sensitivity of P to extremely different patterns of initial soil water content has been

TABLE 4. Portion of convective and stable precipitation.

	Convective fraction (%)	Stable fraction (%)
ClimRAMS	75.98	24.01
CRCM	51.64	48.35
DARLAM	97.65	2.34
EM	66.32	33.67
HIRHAM	39.57	60.42
MM5–ANL	39.62	60.37
MM5–BATS	36.52	63.47
NCEP RSM	60.67	39.32
PROMES	87.73	12.26
RegCM2	N/A	N/A
Scripps RSM	67.88	32.11
SweCLIM-ECMWF	51.75	48.24
SweCLIM-NCEP	46.22	53.77

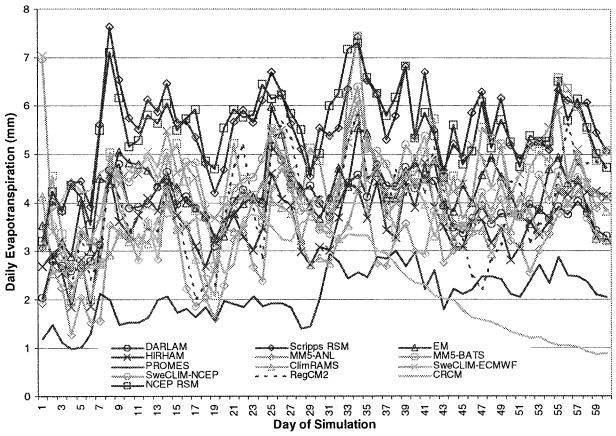

FIG. 2. Time series of daily evapotranspiration (mm) from each RCM.

demonstrated in many RCM simulations of June–July 1993 (Paegle et al. 1996; Giorgi et al. 1996; Seth and Giorgi 1998; Bosilovich and Sun 1999; Hong and Leetmaa 1999; Hong and Pan 2000). Unlike these studies, initial soil water content is nearly saturated in all RCMs with the exception of PROMES and CRCM (see section 2a), neither of which produced *P* notably different from other simulations. There is evidence that *P* and *E* are coupled more strongly in NCEP RSM and Scripps RSM than in the other RCMs of this intercomparison. As will be presented in section 3d, convective precipitation in both RSM simulations peaked during the afternoon when evaporation rate peaked and moisture flux convergence was at its minimum, suggesting that afternoon destabilization by latent heat flux from the land surface scheme directly enhanced *P*. In general, however, rank correspondence of *E* and *P* is not a consistent feature of RCMs in this intercomparison.

Precipitation processes in RCMs are directly related to parameterizations for convective and stable precipitation. To examine whether convective parameterization alone has systematic influence on simulated precipitation, we have calculated the fraction of simulated precipitation that comes from convective and stable parameterizations. The convective portion of model precipitation varies greatly between the simulations, ranging from 97% to 39% (Table 4), although only two RCMs (PROMES and DARLAM) exceed 70% convective fraction. While convective fraction is nearly identical in MM5–ANL and MM5–BATS, in which the Grell convective parameterization scheme is used, there is large variability of convective fraction between different RCMs that use the Kain–Fritsch convective parameterization (SweCLIM, PROMES, and CRCM). This indicates that variability of convective fraction in this intercomparison is RCM-dependent. Despite the wide range of convective fraction, neither linear relation nor rank correspondence is evident between convective fraction and total precipitation.

3) EVAPOTRANSPIRATION (*E*)

Observed *E* is difficult to ascertain, since it is measured in few locations. Trenberth and Guillemot (1996) have estimated that *E* during May–June–July 1993 was $\sim$4 mm day^{-1}, which is nearly equal to estimates of its climatological value (Roads et al. 1994; Berbery and Rasmusson 1999; Gutowski et al. 1997). Kunkel et al. (1994) concluded that potential evapotranspiration during June–July 1993 was slightly less than its climatological value because of enhanced cloudiness. Thus, a climatological value for *E* may be an appropriate estimate for June–July 1993. The RCM-average *E* is 3.9 mm day^{-1}, which is nearly identical to the climatological estimate of 4 mm day^{-1}. Ten RCMs (ClimRAMS, DARLAM, ETH, HIRHAM, MM5–ANL, MM5–BATS, SweCLIM-ECMWF, SweCLIM-NCEP, RegCM2) produce *E* within 15% of the RCM average (Table 3).

The evidence indicates systematic error for extreme values of *E* produced by PROMES (low *E*) and the two RSMs (high *E*). Time series of daily evaporation shows only PROMES and CRCM have an apparent trend of daily evapotranspiration (Fig. 2), whereas daily evapotranspiration appears to fluctuate randomly about *E* in all other RCMs. This occurs despite positive $P - E$ over the period, which would tend to increase the soil moisture content. This suggests that the average soil water content in nearly all RCMs was sufficiently close to saturation so that factors controlling evapotranspiration are likely to be specific to components of land surface schemes used in the RCMs rather than the soil water content itself. The trend in CRCM is directly related to its unique decrease of daily precipitation rate over the midwest United States in the latter half of the simulation period when precipitation systems remained near the northern lateral boundary. In PROMES, an increasing trend of evapotranspiration is evident, suggesting that the initial soil water content had a controlling influence on evapotranspiration during the first 30 days. In support of this assertion, the investigators who submitted PRO-

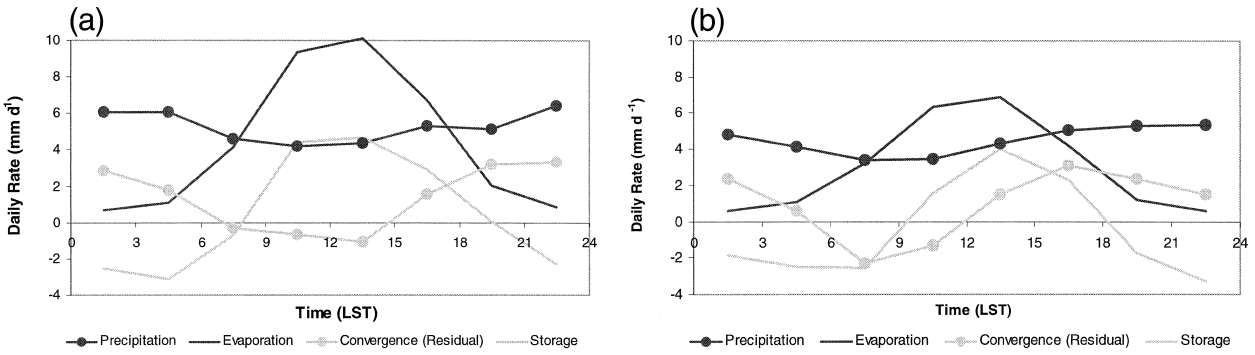

FIG. 3. Daily cycle of terms in the 60-day water vapor conservation equation (1) in (a) group A and (b) group B. RCMs included in group A are: DARLAM, EM, MM5–ANL, MM5–BATS, NCEP RSM, SweCLIM-ECMWF, SweCLIM-NCEP, RegCM2, and Scripps RSM, and in group B are: ClimRAMS, CRCM, HIRHAM, PROMES.

MES also suspect that relatively low E in their simulation is directly related to lower soil water content in the alternative soil moisture initial conditions they used (see section 2a). At the other extreme of E, high values are produced in NCEP RSM and Scripps RSM, despite deriving initial soil conditions from the same source as most of the other RCMs (NCEP–NCAR reanalysis). Betts et al. (1997) reported on tests of an Eta Model implementation (Eta is the primary mesoscale weather forecast model used at NCEP) of the land surface scheme used in both RSMs. They found that this land surface scheme was overly aggressive in drying the upper 10-cm soil layer. In the PIRCS-1b experiment, this behavior could certainly cause an overproduction of E, since soil water content was replenished rapidly in both RSMs as a result of persistent rainfall, and accumulated incident shortwave radiation was higher in these RCMs than in others.

c. Water cycling

Climatological estimates of summertime ρ in the central United States range from 0.15 to 0.25 (Brubaker et al. 1993; Eltahir and Bras 1996; Trenberth 1999), reflecting the strong low-level water vapor transport that characterizes this region's summertime hydrology. Dirmeyer and Brubaker (1999) have estimated that ρ in the central United States during June–July 1993 was within the range 0.05–0.10. The decrease from its climatological value is due to intensified low-level moisture flux (Trenberth and Guillemot 1996). All RCMs produce ρ within the estimated observed range, except PROMES for which ρ is less than the minimum of the estimated observed range (Table 3). The low value of ρ in PROMES is caused by low E, which occurs despite its relatively high insolation. The agreement between the range of ρ in the RCMs and observations further suggests the collective dry bias is due to internal RCM precipitation processes rather than difference in water vapor supply.

d. Daily cycle of water vapor conservation equation (1)

A unique feature of the atmospheric hydrologic cycle of the central United States is dependence of precipitation on nocturnal water vapor flux convergence. This feature is absent in the NCEP–NCAR reanalysis data (Higgins et al. 1997) that is used to drive many of the local-area models in PIRCS-1b. We constructed daily cycles of terms of the water vapor conservation equation (1) in order to determine whether the RCMs had simulated temporal separation between maximum evapotranspiration and maxima of precipitation and convergence. We found that daily cycles of C and P exhibited nocturnal maxima in most but not all RCMs. We formed two subgroups and computed composite daily cycles of water conservation components to illustrate this distinction. Group A is composed of the nine RCMs (DARLAM, EM, MM5–ANL, MM5–BATS, NCEP RSM, SweCLIM-ECMWF, SweCLIM-NCEP, RegCM2, Scripps RSM) for which daily cycles of P and C both contained a nocturnal peak. The remaining four RCMs (ClimRAMS, CRCM, HIRHAM, PROMES) formed group B. (The daily cycle for each RCM may be viewed at www.pircs.iastate.edu/hydrology/watercycle.html.) In general, maxima in the composite daily cycles are smaller in amplitude and broader over time than in any individual model; nevertheless, both composites retain distinctions noted above (Fig. 3).

These results indicate that many of the RCMs in this intercomparison simulate physical details of the atmospheric hydrologic cycle that are absent in the driving data. To examine whether such features are produced by similar mechanisms in different RCMs, we constructed daily cycles of convective and stable precipitation, which are sensitive to different model processes. In all RCMs but ClimRAMS the convective parameterization scheme is invoked by mechanisms related to potential instability in a single model column of an idealized parcel lifted from near the ground. The Kuo convective parameterization scheme in ClimRAMS is more

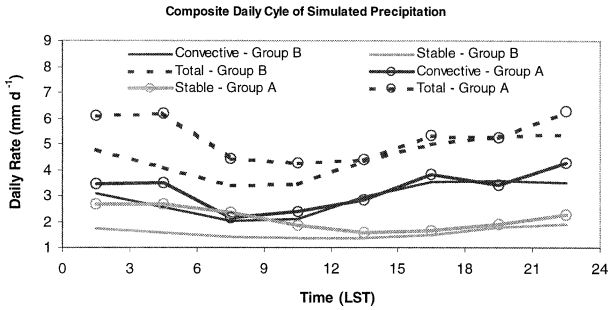

FIG. 4. Daily cycle of simulated 60-day convective, stable, and total precipitation (sum of convective and stable). Members of group A and group B are listed in Fig. 3 caption.

sensitive to moisture flux convergence. Stable precipitation occurs in all RCMs when threshold values of gridpoint relative humidity are exceeded. Thus, in these RCMs convective precipitation reflects a response to destabilization while stable precipitation relates to grid-scale moistening.

We found that daily cycles of convective precipitation for members of group A contain similar trends that are summarized well in the daily cycle of composite convective precipitation (Fig. 4). Convective precipitation in all RCMs of group A except DARLAM was largest at 2230 LST and remained high through 0430 LST. The relatively large value of composite convective precipitation at 1630 LST is caused by DARLAM, which has an extraordinary pattern of maxima at 1630, 2230, and 0430 LST. Stable precipitation for all members of group A peaked overnight between 0130 and 0730 LST (Fig. 4). Because these maxima occur at night, they provide strong indication that both subgrid and grid-scale precipitation in these RCMs was linked to widespread moistening and destabilization by the development of nocturnal moisture flux convergence.

Feedback between surface latent heat flux and precipitation is evident in some RCMs of group A. A gradual increase of composite P occurs during 1030–2230 LST (Fig. 3a). This is due to secondary afternoon maximum of P in Scripps RSM, NCEP RSM, and EM. During this time convective precipitation reaches a secondary maximum, while C is at its minimum in all three RCMs. These results suggest afternoon convective precipitation forms in response to destabilization by surface latent and sensible heat flux in these RCMs.

The daily cycle of composite convective precipitation of group B shows a very different trend from that of group A (Fig. 3b), increasing more rapidly between 1030 and 1630 LST and decreasing after 2230 LST. This broad maximum is caused by variability of the time of maximum convective precipitation. Daily cycles in ClimRAMS and PROMES have a broad maximum, peaking at 1930 LST. A broad maximum occurs slightly later in CRCM from 2230 through 0130 LST. In contrast, HIRHAM has maximum convective precipitation midday at 1330 LST. In PROMES and ClimRAMS maximum convective precipitation occurs simultaneously with maximum C, whereas the time of maximum convective precipitation leads that of C in HIRHAM and CRCM. These results indicate that daytime precipitation in HIRHAM and CRCM is driven by destabilization from surface latent heat flux, but in PROMES and ClimRAMS the influence of surface latent heat flux cannot be separated from that of moisture flux convergence.

Composite stable precipitation for group B has a broad nocturnal maximum, but the amplitude of its diurnal cycle is much smaller than in the composite of group A (Fig. 3b). Only ClimRAMS and CRCM have simultaneous maxima of stable precipitation and C. These maxima occur at 1630 (ClimRAMS) and 1930 (CRCM), however, rather than overnight as in the RCMs of group A.

Daily cycles of F'_{in} and F'_{out} were constructed to further examine differences in timing of maximum C (moisture flux fields were unavailable for ClimRAMS, CRCM, and MM5–ANL). In all RCMs the time of maximum F'_{in} occurs at 0000 LST, which is the time of peak LLJ frequency in all RCMs and near the time of peak LLJ frequency in hourly National Oceanic and Atmospheric Administration (NOAA) wind profiler data (Fig. 5; Arritt et al. 1997). However, the magnitude of the nocturnal maximum is larger for RCMs of group A than for HIR-

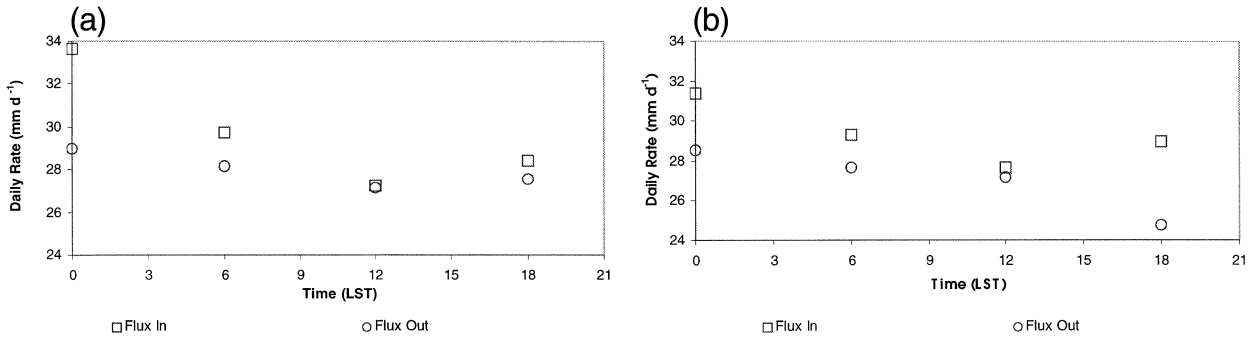

FIG. 5. Daily cycle of 60-day water vapor influx and efflux in (a) group A and (b) group B. Members of group A and group B are listed in Fig. 3 caption.

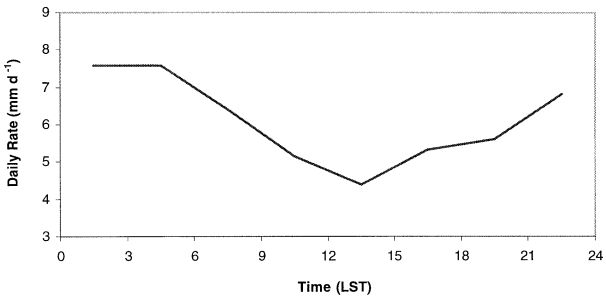

FIG. 6. Daily cycle of 60-day precipitation in station reports.

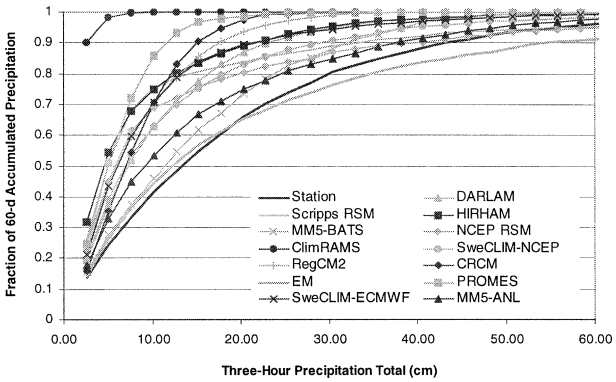

FIG. 7. Frequency of 3-h precipitation totals expressed as a cumulative fraction of 60-day accumulated precipitation.

HAM and PROMES, which leads to greater nocturnal convergence in RCMs of group A. Since maximum F'_{in} is related to LLJ frequency, it is also related to the dynamic evolution of LLJs, which contains a substantial divergent (ageostrophic) component (Blackadar 1957; Uccellini and Johnson 1979; Chen and Kpaeyeh 1993). One plausible explanation for the disparity in amplitude of the diurnal cycle of F'_{in} might be the magnitude of horizontal diffusion used to ensure computational stability. Greater diffusion would tend to reduce the magnitude of moisture flux, especially the divergent component.

The daily cycle of F'_{out} is very similar in all RCMs, except at 1800 LST when F'_{out} for HIRHAM and PROMES is greatly reduced compared to F'_{out} in RCMs of group A, thereby creating afternoon convergence. This behavior is atypical compared not only with the other RCMs in this intercomparison but also with climatological studies of LLJs and moisture transport (Higgins et al. 1997).

e. Daily cycle of observed precipitation

The daily cycle of station P contains a single nocturnal maximum during 0130–0430 LST and sharp decrease during 0430–1330 LST (Fig. 6). These features resemble those of the climatological daily cycle for precipitation in Iowa (Takle 1995), though the amplitude of the daily cycle in 1993 is larger. The timing of maximum P in group A is much closer to the observed time of maximum P than in group B. This further suggests that the relationship between the large-scale circulation and precipitation is incorrectly simulated by members of group B. Moreover, three members of group B (ClimRAMS, HIRHAM, CRCM) rank as the three driest RCMs of this collection, suggesting that incorrectly relating precipitation to the resolvable-scale circulation affects not only the daily cycle of precipitation but also time-average water conservation.

f. 3-h precipitation totals

1) HISTOGRAM OF 3-H PRECIPITATION TOTALS

Heavy precipitation events were unusually frequent during the peak flood period in late June and early July 1993 (Kunkel et al. 1994). Such events were mesoscale in nature, so that the ability of RCMs to simulate heavy mesoscale precipitation events is an important indicator of whether they add information to large-scale analyses or GCM output. Evidence that RCMs can add physical detail to large-scale analyses was given by Takle et al. (1999), who show that many RCMs in PIRCS experiment 1a produced a large MCS under conditions of weak synoptic forcing. Here, we examine statistics of 3-h precipitation totals, which is influenced by the integrated effect of localized heavy precipitation events and MCS. Station precipitation is accumulated over 3-h intervals identical to the archived intervals of the RCMs. The lowest observable precipitation amount (2.54 mm) determined the lowest 3-h total and bin increment in the histograms (see section 2b). Histograms were expressed in precipitation units (mm) by multiplying counts with 3-h total.

In Fig. 7 cumulative histograms for each dataset are normalized by 60-day accumulated precipitation. All curves of cumulative fraction in RCMs except EM lie to the left of the observed curve. This means that a larger fraction of 60-day accumulated precipitation in the RCMs is produced by lower 3-h totals than is observed. For example, the fraction that is produced by 3-h totals $\leq$12.70 mm is larger in all RCMs than in the station data. Our interest is in heavy precipitation for which there do not exist widely accepted, objective thresholds. We define ''heavy 3-h precipitation'' as those 3-h rates that contribute the upper 10% of 60-day accumulated precipitation for each dataset. By this definition heavy 3-h precipitation contributes equally to 60-day accumulated precipitation in the simulations and station data, but the threshold that defines heavy 3-h precipitation may vary. In fact, thresholds under this definition range from 2.54 mm (ClimRAMS) to 53.34 mm (EM), although 8 of 13 RCMs are within a smaller range of 10.16–35.56 mm. Thresholds for the simulations are generally lower than for the station data (43.18 mm). Simulations with severe dry bias tended to produce lower thresholds (ClimRAMS, HIRHAM, CRCM)

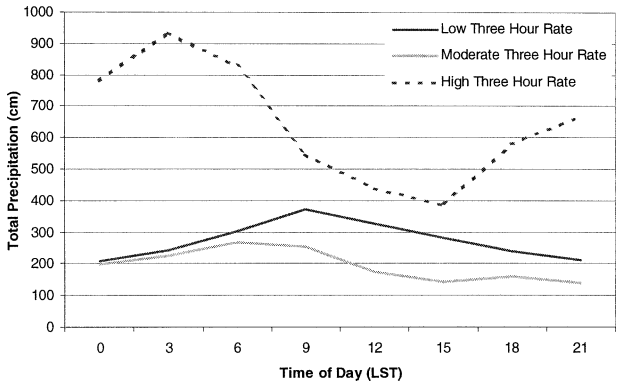

FIG. 8. Daily cycle of accumulated precipitation for high (12.70–101.60 mm), moderate (7.62–10.16 mm), and low (2.54–5.08 mm) 3-h precipitation totals in station reports.

compared with other RCMs, whereas simulations in which the threshold was similar to that observed (DARLAM, EM, MM5–ANL, NCEP RSM, Scripps RSM) tended to have either high value of *P* or large magnitude of regional maximum precipitation in their precipitation field.

The tendency for models to produce more precipitation than observed at low precipitation rates is reported for many different timescales in many climate simulations (Giorgi et al. 1996; Kunkel et al. 2002). An explanation for this tendency is that different horizontal scales are represented by precipitation in station data and RCMs. Rain gauge measurements are point observations (Legates and Willmot 1990), whereas the RCMs in this intercomparison cannot resolve processes having horizontal scale smaller than several times their nominal grid spacing of 50 km. The important finding herein is not that these RCMs produced more precipitation at lower than observed precipitation rates. Instead, the results indicate that inadequacy in representing heavy 3-h precipitation totals and overproducing low 3-h precipitation totals has resulted in a tendency toward dry bias.

More recent work with ClimRAMS (version 4.3) has introduced the Kain–Fritsch (KF) cumulus parameterization scheme as an alternative to the Kuo schemed used in the PIRCS study. Preliminary RAMS-KF simulations improve the low-precipitation biases, especially in the central United States (Castro et al. 2001). Results with RAMS-KF will be presented in a future paper on the North American Monsoon Model Intercomparison Project (NAMIP).

2) DAILY CYCLE OF FREQUENCY OF 3-H TOTALS

In the station data, different daily cycles of accumulated 3-h totals were found for ranges of 3-h totals of 2.54–5.08, 7.62–10.16, and 12.70–101.60 mm. We defined low, moderate, and high 3-h total categories corresponding to these 3-h total ranges. We applied the same categorical analysis to the simulations. Arguably, 3-h total ranges should be redefined because of the disparity between station and RCM climatologies. However, high-rate precipitation is well defined by 3-h totals $\geq$12.70 mm for all but one simulation. To associate meteorological features with the daily cycles, we examined cloud-top characteristics in *GOES-8* IR imagery.

Daily cycles of accumulated precipitation in each category in the station data have a single peak, but the peak accumulation of high 3-h totals occurs at 0900 LST, while for moderate and low 3-h totals the peaks occur at 1200 and 1500 LST, respectively (Fig. 8). Widespread high 3-h totals are associated with mature MCSs in *GOES-8* IR imagery, whereas low 3-h totals are associated with either the decay of an MCS or (less often) coverage by low-level stratus clouds. Therefore, the time shift of maximum accumulated precipitation is associated with the frequent development and decay of nocturnal MCSs within the UMRB box.

In the RCM simulations, daily cycles of the accumulations for low, moderate, and high 3-h totals each contain a single peak (except in DARLAM; Fig. 9). In the composite of group A, accumulated precipitation

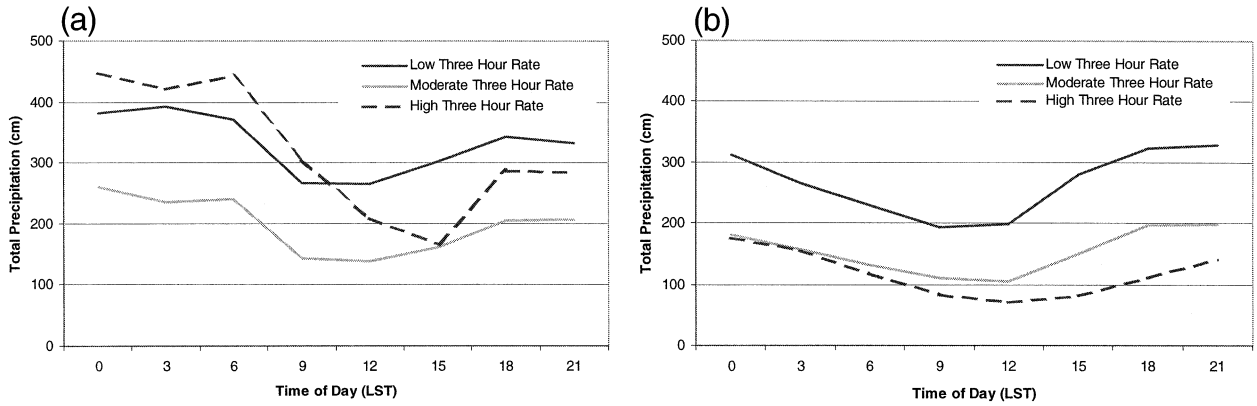

FIG. 9. Daily cycle of accumulated precipitation for high (12.70–101.60 mm), moderate (7.62–10.16 mm), and low (2.54–5.08 mm) 3-h precipitation totals in (a) group A and (b) group B. Members of group A and group B are listed in Fig. 3 caption.

from high 3-h totals peaks overnight. (The daily cycle for each simulation may be viewed on the PIRCS Web page at www.pircs.iastate.edu/hydrology/daily/threehourtotals.html.) Accumulated precipitation from moderate and low 3-h totals peaks simultaneously with high 3-h totals. In the composite of group B, maximum accumulation from low and moderate 3-h totals is greater than and *leads* that of high 3-h totals. (Recall that the peak accumulation of low 3-h totals *lagged* that of high 3-h totals in station data.) Thus, daily cycles of 3-h totals in all simulations lack a lagged-correlation signal that is consistent with that of observed, recurrent MCSs, suggesting that the RCMs do not properly simulate MCS development and decay.

4. Summary and discussion

We have compared output from 13 RCM simulations of the central United States flood of June–July 1993 with each other and observations. Our comparison focused on identifying systematic differences in the atmospheric water cycle over the portion of the upper Mississippi River basin where flooding was most intense. Following are the main results of this intercomparison:

- All RCM simulations produced a precipitation maximum in the upper Mississippi River basin. In 10 out of 13 RCMs maximum precipitation occurred northeast of observed maximum precipitation. Maps of 60-day average near-surface potential temperature and LLJ frequency strongly suggested that a primary precipitation mechanism in these RCMs was frontal overrunning. Maximum values of simulated precipitation fields enveloped the observed maximum and ranged from 325 to just over 700 mm.
- All RCM simulations produced $P - E > 0$, but in only DARLAM and PROMES was $P - E$ as large as estimates of observed $P - E$; the general tendency to understate $P - E$ was caused by low bias of P that ranged 0.2 to 2.0 mm day^{-1}.
- RCM values for E were not consistently greater than or less than estimated values of observed E. Extreme values of E were caused by biases in subcomponents of individual RCMs; systematic influences could not be identified for RCMs with E in the range of 3.3–4.3 mm day^{-1}.
- Nine of thirteen RCMs produced qualitatively similar daily cycles of the terms of the water vapor conservation equation (1) in which maximums of P and C occurred simultaneously at night; in the other four RCMs consistent relation between maximums of P and C were not found, even though maximum P occurred during afternoon in all four RCMs.
- RCMs with dry bias had excessive frequency of low 3-h precipitation totals and very low frequency of high 3-h totals.
- All RCMs failed to emulate a time lag between maximum accumulation of high 3-h precipitation totals and low 3-h precipitation totals that was observed in station precipitation and was caused by precipitation from MCSs.

A key indicator of the potential of RCMs in this intercomparison to add realistic hydroclimatological detail is the ability of most RCMs to simulate a nocturnal maximum of precipitation. This feature is absent in the NCEP–NCAR reanalysis climatology (Higgins et al. 1997). In fact, global climate models and reanalyses, which typically have been run at horizontal node spacing much coarser than the RCM simulations analyzed herein, usually do not exhibit nocturnal maximum of precipitation (Ghan et al. 1996; Higgins et al. 1997).

Additional tests are needed to determine whether more detail may be accurately simulated. Even though there is evidence that very large MCSs may be simulated by RCMs (Takle et al. 1999), the absence of a realistic MCS signal in RCM precipitation suggests that many systems are simulated incorrectly. Although the dynamical scale of such systems may be at or slightly less than the Rossby radius of deformation (Zhang and Fritsch 1987; Cotton et al. 1989), it is important to simulate such mesoscale dynamics of climate correctly in order to have confidence in simulations made as forecasts. In simulations of June–July 1993 it likely is necessary to do so in order to correctly reproduce the location of maximum precipitation. Mesoscale models that have reproduced many of the dynamical features of MCSs (Zhang and Fritsch 1987; Stensrud and Fritsch 1994) generally use node spacing that is at most one-half of the spacing of RCMs in this intercomparison, suggesting that a first step might be sensitivity analysis of PIRCS experiment 1b results to horizontal node spacing.

In addition to short-period tests designed to examine RCM processes, intercomparisons are needed over extended periods to determine whether RCM simulations produce accurate hydroclimatology. Results from PIRCS-1a, in which RCM simulations of an extreme drought in the central United States were performed, indicated a common tendency of simulated precipitation to be larger than observed. Thus, when combined with the tendency of RCMs in PIRCS-1b to underestimate precipitation, these experiments suggest the possibility that RCMs will underestimate the magnitude of extreme hydrological anomalies. A potential consequence is that long-period simulations may contain damped interannual variability. Simulations spanning multiple decades are needed to test this possibility.

Acknowledgments. This research was sponsored in part by National Science Foundation Grants ATM-9909650, ATM-9911417, and ATM-0121028; United States National Oceanic and Atmospheric Administration Grants NA86GP0572 and NA16GP1583; the Office of Biological and Environmental Research, U. S. De-

partment of Energy, under Contract W-31-109-ENG-38; and the BER Program of DOE through NIGEC under Cooperative Agreement DE-FC03-90ER61010. This is Journal Paper Number J-19553 of the Iowa Home Economics and Experiment Station Project 3803.

REFERENCES

Anderson, C. J., and R. W. Arritt, 1998: Mesoscale convective complexes and persistent elongated convective systems over the United States during 1992 and 1993. *Mon. Wea. Rev.,* **126,** 578–599.

Arakawa, A., and W. Schubert, 1974: Interaction of a cumulus cloud ensemble with the large-scale environment. *J. Atmos. Sci.,* **31,** 674–701.

Arritt, R. W., T. D. Rink, M. Segal, D. P. Todey, C. A. Clark, M. J. Mitchell, and K. M. Labas, 1997: The Great Plains low-level jet during the warm season of 1993. *Mon. Wea. Rev.,* **125,** 2176–2192.

Barnes, S. L., 1964: A technique for maximizing details in numerical weather map analysis. *J. Appl. Meteor.,* **3,** 396–409.

Berbery, E. H., and E. M. Rasmusson, 1999: Mississippi moisture budgets on regional scales. *Mon. Wea. Rev.,* **127,** 2654–2673.

Betts, A. K., F. Chen, K. E. Mitchell, and Z. I. Janjic, 1997: Assessment of the land surface and boundary layer models in two operational versions of the NCEP Eta Model using FIFE data. *Mon. Wea. Rev.,* **125,** 2896–2916.

Blackadar, A. K., 1957: Boundary layer wind maxima and their significance for the formation of nominal inversions. *Bull. Amer. Meteor. Soc.,* **38,** 283–290.

Bosilovich, M. G., and W.-Y. Sun, 1999: Numerical simulation of the 1993 midwestern flood: Land–atmosphere interactions. *J. Climate,* **12,** 2490–2505.

Brubaker, K. L., D. Entekhabi, and P. S. Eagleson, 1993: Estimation of continental precipitation recycling. *J. Climate,* **6,** 1077–1089.

Burde, G. I., and A. Zangvil, 2001: The estimation of regional precipitation recycling. Part I: Review of recycling models. *J. Climate,* **14,** 2497–2508.

Castro, C. L., R. A. Pielke Sr., and G. E. Liston, 2001: Simulation of North American monsoon in different Pacific SST regimes using RAMS. *Proc. 26th Annual Climate Diagnostics and Prediction Workshop,* La Jolla, CA, Scripps Institution of Oceanography and the Climate Prediction Center.

Caya, D., and R. Laprise, 1999: A semi-Lagrangian semi-implicit regional climate model: The Canadian RCM. *Mon. Wea. Rev.,* **127,** 341–362.

Chen, F., and J. Dudhia, 2001: Coupling an advanced land-surface–hydrology model with the Penn State–NCAR MM5 modeling system. Part I: Model implementation and sensitivity. *Mon. Wea. Rev.,* **129,** 569–585.

Chen, T.-C., and J. A. Kpaeyeh, 1993: The synoptic-scale environment associated with the low-level jet of the Great Plains. *Mon. Wea. Rev.,* **121,** 416–420.

Christensen, J. H., B. Machenhauer, R. G. Jones, C. Schar, P. Ruti, M. Castro, and G. Visconti, 1997: Validation of present-day regional climate simulations over Europe: LAM simulations with observed boundary conditions. *Climate Dyn.,* **13,** 489–506.

Cotton, W. R., M.-S. Lin, R. L. McAnnelly, and C. J. Tremback, 1989: A composite model of mesoscale convective complexes. *Mon. Wea. Rev.,* **117,** 765–783.

Davies, H. C., 1976: A lateral boundary formulation for multi-level prediction models. *Quart. J. Roy. Meteor. Soc.,* **102,** 405–418.

Dickinson, R. E., A. Henderson-Sellers, and P. J. Kennedy, 1993: Biosphere–Atmosphere Transfer Scheme (BATS) version 1E as coupled to the NCAR Community Climate Model. Tech. Note NCAR/TN-387+STR, National Center for Atmospheric Research, Boulder, CO, 72 pp.

Dirmeyer, P. A., and K. L. Brubaker, 1999: Contrasting evaporative moisture sources during the drought of 1988 and the flood of 1993. *J. Geophys. Res.,* **104,** 19 383–19 397.

Elathir, E. A. B., and L. B. Bras, 1996: Precipitation recycling. *Rev. Geophys.,* **34,** 367–378.

Fritsch, J. M., R. J. Kane, and C. R. Chelius, 1986: The contribution of mesoscale convective weather systems to the warm-season precipitation in the United States. *J. Climate Appl. Meteor.,* **25,** 1333–1345.

Gaertner, M. A., O. B. Christensen, J. A. Prego, J. Polcher, C. Gallardo, and M. Castro, 2001: The impact of deforestation on the hydrologic cycle in the western Mediterranean: An ensemble study with two regional models. *Climate Dyn.,* **17,** 857–873.

Ghan, S. J., X. Bian, and L. Corsetti, 1996: Simulation of the Great Plains low-level jet and associated clouds by general circulation models. *Mon. Wea. Rev.,* **124,** 1388–1408.

Giorgi, F., and L. O. Mearns, 1999: Introduction to special section: Regional climate modeling revisited. *J. Geophys. Res.,* **104,** 6335–6352.

——, M. R. Marinucci, and G. T. Bates, 1993a: Development of a second-generation regional climate model (Regcm2). Part I: Boundary-layer and radiative transfer processes. *Mon. Wea. Rev.,* **121,** 2794–2813.

——, ——, G. DeCanio and G. T. Bates, 1993b: Development of a second-generation regional climate model (Regcm2). Part II: Convective processes and assimilation of lateral boundary conditions. *Mon. Wea. Rev.,* **121,** 2814–2832.

——, L. O. Mearns, C. Shields, and L. Mayer, 1996: A regional model study of the importance of local versus remote controls of the 1988 drought and 1993 flood over the central United States. *J. Climate,* **9,** 1150–1162.

Grell, G. A., 1993: Prognostic evaluation of assumptions used by a cumulus parameterization. *Mon. Wea. Rev.,* **121,** 764–787.

——, J. Dudhia, and D. R. Stauffer, 1993: A description of the fifth-generation Penn State/NCAR mesoscale model (MM5). NCAR Tech. Note NCAR/TN-397+STR. National Center for Atmospheric Research, Boulder, CO, 200 pp.

Gutowski, W. J., Jr., Y. Chen, and Z. Otles, 1997: Atmospheric water vapor transport in NCEP–NCAR reanalyses: Comparison with river discharge in the central United States. *Bull. Amer. Meteor. Soc.,* **78,** 1957–1969.

——, E. S. Takle, and R. W. Arritt, 1998: Project to intercompare regional climate simulations, Workshop II, 5–6 June 1997. *Bull. Amer. Meteor. Soc.,* **79,** 657–659.

Higgins, R. W., K. C. Mo, and S. D. Schubert, 1996: The moisture budget of the central United States in spring as evaluated in the NCEP/NCAR and the NASA/DAO reanalyses. *Mon. Wea. Rev.,* **124,** 939–963.

——, Y. Yao, E. S. Yarosh, J. E. Janowiak, and K. C. Mo, 1997: Influence of the Great Plains low-level jet on summertime precipitation and moisture transport over the central United States. *J. Climate,* **10,** 481–507.

Holtslag, A. A. M., E. I. F. de Bruijn, and H. L. Pan, 1990: A high-resolution airmass transformation model for short-range weather forecasting. *Mon. Wea. Rev.,* **118,** 1561–1575.

Hong, S.-Y., 2000: Impact of the subgrid representation of parameterized convection on simulated climatology. NCEP Office Note 428, 32 pp. [Available from NOAA/NWS/NCEP, Environmental Modeling Center, WWB, Room 207, Washington, DC 20233.]

——, and H.-L. Pan, 1996: Nonlocal boundary layer vertical diffusion in a medium-range forecast model. *Mon. Wea. Rev.,* **124,** 2322–2339.

——, and A. Leetmaa, 1999: An evaluation of the NCEP RSM for regional climate modeling. *J. Climate,* **12,** 592–609.

——, and H.-L. Pan, 2000: Impact of soil moisture anomalies on seasonal summertime circulation over North America in a regional climate model. *J. Geophys. Res.,* **105** (D24), 29 625–29 634.

Jones, C., and U. Willen, 2001: The diurnal cycle of clouds and precipitation. *Proc. Third Study Conf. on BALTEX,* Marinehann, Finland, European Commission, 101–103.

Juang, H.-M. H., and M. Kanamitsu, 1994: The NMC nested regional spectral model. *Mon. Wea. Rev.,* **122,** 3–26.

——, and S.-Y. Hong, 2001: Sensitivity of the NCEP regional spectral model on domain size and nesting strategy. *Mon. Wea. Rev.,* **129,** 2904–2922.

——, ——, and M. Kanamitsu, 1997: The NCEP regional spectral model: An update. *Bull. Amer. Meteor. Soc.,* **78,** 2125–2143.

Junker, N. W., R. S. Schneider, and S. L. Fauver, 1999: A study of heavy rainfall events during the great Midwest flood of 1993. *Wea. Forecasting,* **14,** 701–712.

Kain, J. S., and J. M. Fritsch, 1990: A one-dimensional entraining/detraining plume model and its application in convective parameterization. *J. Atmos. Sci.,* **47,** 2784–2802.

Kunkel, K. E., 1990: Operational soil moisture estimation for the midwestern United States. *J. Appl. Meteor.,* **29,** 1158–1166.

——, S. A. Changnon, and J. R. Angel, 1994: Climatic aspects of the 1993 upper Mississippi River Basin. *Bull. Amer. Meteor. Soc.,* **75,** 811–822.

——, K. Andsager, X.-Z. Liang, R. W. Arritt, E. S. Takle, W. J. Gutowski Jr., and Z. Pan, 2002: Observations and regional climate model simulations of heavy precipitation events and seasonal anomalies: A comparison. *J. Hydrometeor.,* **3,** 322–334.

Kuo, H. L., 1974: Further studies of the parameterization of the influence of cumulus convection on large-scale flow. *J. Atmos. Sci.,* **31,** 1232–1240.

Lakhtakia, M. N., and T. T. Warner, 1994: A comparison of simple and complex treatments of surface hydrology and thermodynamics suitable for mesoscale atmospheric models. *Mon. Wea. Rev.,* **122,** 880–896.

Legates, D. R., and C. J. Willmot, 1990: Mean seasonal and spatial variability in gauge-corrected global precipitation. *Int. J. Climatol.,* **10,** 111–127.

Liston, G. E., and R. A. Pielke Sr., 2001: A climate version of the regional atmospheric modeling system. *Theor. Appl. Climatol.,* **68,** 155–173.

Lüthi, D., A. Cress, H. C. Davis, C. Frei, and C. Shär, 1996: Interannual variability and regional climate simulations. *Theor. Appl. Climatol.,* **53,** 185–209.

McGregor, J. L., and K. J. Walsh, 1994: Climate change simulations of Tasmanian precipitation using multiple nesting. *J. Geophys. Res.,* **99,** 20 889–20 905.

——, H. B. Gordon, I. G. Watterson, M. R. Dix, and L. D. Rotstayn, 1993a: The CSIRO 9-level atmospheric general circulation model. CSIRO Division of Atmospheric Research Tech. Paper 26, 89 pp.

——, K. J. Walsh, and J. J. Katzfey, 1993b: Nested modeling for regional climate studies. *Modeling Change in Environmental Systems,* A. J. Jakeman et al., Eds., John Wiley, 367–386.

Paegle, J., K. C. Mo, and J. Nogues-Paegle, 1996: Dependence of simulated precipitation on surface evaporation during the 1993 United States summer floods. *Mon. Wea. Rev.,* **124,** 345–361.

Pan, H.-L., and W.-S. Wu, 1995: Implementing a mass flux convective parameterization package for the NMC medium-range forecast model. NMC Office Note 409, 40 pp. [Available from NOAA/NWS/NCEP, Environmental Modeling Center, WWB, Room 207, Washington, DC 20233.]

Peixoto, J. P., and A. H. Oort, 1992: *Physics of Climate.* American Institute of Physics, 520 pp.

Pielke, R. A., Sr., and Coauthors, 1992: A comprehensive meteorological modeling system—RAMS. *Meteor. Atmos. Phys.,* **49,** 69–91.

Rasmusson, E. M., 1967: Atmospheric water vapor transport and the balance of North America: Part I. Characteristics of the water vapor field. *Mon. Wea. Rev.,* **95,** 403–426.

——, 1968: Atmospheric water vapor transport and the balance of North America: Part II. Large-scale water balance investigations. *Mon. Wea. Rev.,* **96,** 720–734.

Roads, J. O., S.-C. Chen, A. K. Guetter, and K. P. Georgakakis, 1994: Large-scale aspects of the United States hydrologic cycle. *Bull. Amer. Meteor. Soc.,* **75,** 1589–1610.

Seth, A., and F. Giorgi, 1998: The effects of domain choice on summer precipitation simulation and sensitivity in a regional climate model. *J. Climate,* **11,** 2698–2712.

Stensrud, D. J., and J. M. Fritsch, 1994: Mesoscale convective systems in weakly forced large-scale environments. Part III: Numerical simulations and implications for operational forecasting. *Mon. Wea. Rev.,* **122,** 2084–2104.

Takle, E. S., 1995: Variability of midwest summertime precipitation. *Preparing for Global Change: A Midwestern Perspective,* G. R. Carmichael et al., Eds., SPB Academic, 43–59.

——, and Coauthors, 1999: Project to intercompare regional climate simulations (PIRCS): Description and initial results. *J. Geophys. Res.,* **104,** 19 433–19 461.

Taylor, J. A., and J. W. Larson, 2001: Resolution dependence in modeling extreme weather events. *Computational Science—ICCS 2001: Proceedings, Part I,* V. N. Alexandrov et al., Eds., Lecture Notes in Computer Science, Vol. 2073, Springer-Verlag, 204–211.

Tiedtke, M., 1989: A comprehensive mass flux scheme for cumulus parameterization in large-scale models. *Mon. Wea. Rev.,* **117,** 1779–1800.

Trenberth, K. E., 1999: Atmospheric moisture recycling: Role of advection and local evaporation. *J. Climate,* **12,** 1368–1381.

——, and C. J. Guillemot, 1996: Physical processes involved in the 1988 drought and 1993 floods in North America. *J. Climate,* **9,** 1288–1298.

Troen, I., and L. Mahrt, 1987: A simple model of the atmospheric boundary layer: Sensitivity to surface evaporation. *Bound.-Layer Meteor.,* **37,** 129–148.

Uccellini, L. W., and D. R. Johnson, 1979: The coupling of upper and lower tropospheric jet streaks and implications for the development of severe convective storms. *Mon. Wea. Rev.,* **107,** 682–703.

Wallace, J. M., 1975: Diurnal variations in precipitation and thunderstorm frequency over the conterminous United States. *Mon. Wea. Rev.,* **103,** 406–419.

Zhang, D.-L., and R. A. Anthes, 1982: A high-resolution model of the planetary boundary layer—Sensitivity tests and comparisons with SESAME-79 data. *J. Appl. Meteor.,* **21,** 1594–1609.

——, and J. M. Fritsch, 1987: Numerical simulation of the meso-β scale structure and evolution of the 1977 Johnstown flood. Part II: Inertially stable warm-core vortex and the mesoscale convective complex. *J. Atmos. Sci.,* **44,** 2593–2612.